Opto-Electronic Engineering

Article

2017, Vol 44, Issue 1

Splitting light beam by meanderline with continuous phase profile

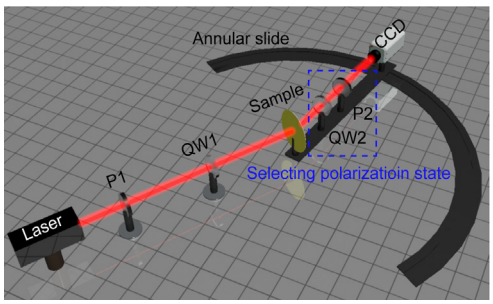

Min Wang*, Kun Song, Jianyuan Wang and Kexin Jin

School of Natural and Applied Sciences, Northwestern Polytechnical University, Xi'an 710072, China

Abstract: It has been successfully demonstrated can be widely used in nano-photonics applications owing to their flexible wavefront manipulation in a limited physical profile. However, how to improve the efficiency for the transmission light is still a challenge. We experimentally demonstrate that the sine-shaped metallic meanderline fabricated by focus ion beam technology converts circularly polarized (CP) light to its opposite handedness and sends them into different propagation directions depending on the polarization states in near-infrared and visible frequency regions. The beam splitting behavior is well characterized by a simple geometry relation, following the rule concluded from other works on the wavefront manipulation of metasurface with phase discontinuity. Importantly, the meanderline is demonstrated to be more efficient in realizing the same functions due to the suppressed high order diffractions resulted from the absence of interruption in phase profile. The theoretical efficiency reaches 67%. Particularly, potential improvements are feasible by changing or optimizing shape of the meanderline, offering high flexibility in applications for optical imaging, communications and other phase-relative techniques. Additionally, since the continuous phase provided by the meanderline can improve the sampling efficiency of the phase function, it is helpful in realizing high quality hologram.

Keywords: electromagnetic wave; metamaterials; super-resolution; flat lens; absorber

DOI: 10.3969/j.issn.1003-501X.2017.01.011 **Citation:** *Opto-Elec Eng*, 2017, **44**(1): 97–102

1 Introduction

Beam splitter which divides an input beam into several output beams plays a fundamental role in optical applications, such as interference-optic, optic communication, and laser physics. Classical devices encompassing glued prisms, birefringent materials and coated mirrors, split beam suffered from transmittance or anisotropic feature of the material, leading to inherent drawbacks of profile dimension or/and narrowband response[1]. With the development of diffraction optics[2], new types of the beam splitter are fostered including binary grating and holographic grating. Diffraction optical elements usually have narrow operation bandwidth due to the phase-dependent nature, albeit a revolution in micro-optics. Meanwhile, at least one half-wavelength is required to accumulate enough phase change for such devices. In a word, these devices are generally limited in miniaturized and integrated modern nano-photonics applications. In the recent, metasurfaces had been successfully demonstrated to break the thickness limitation owing to the deep-subwavelength-dimension elements both in horizontal and vertical directions[3].

In 2011, F. Capasso et al. demonstrated that arbitrarily abrupt phase can be obtained by spatially tailoring the geometry or orientation of the V-shaped nanoresonator[4]. Metasurfaces composed of such elements show capacities of anomalous light bend and optical vortices generation. Later, other elements including nanorods[5-7], nanoslits[8-10], L-shaped[11] or other nanostructures[12-15], were put forward to tailor the phase[16-21]. Flexible phase profile reconstructions open opportunities for metasurfaces in applications of ultrathin flat metalens[22-24], beam shaper[25-26], quarter-wave plate[27], optical holography[28-31], etc[32-35]. Methods for designing metasurfaces and analyzing the behaviors of electromagnetic wave in metasurfaces are well described in the literatures[36-37].

Nevertheless, some unavoidable drawbacks still exist. On one hand, in order to efficiently tailor the light wavefront, pixel of the metasurface should be as high as possible, which would bring more rigorous fabrication requirements. The literature reported in 2013 demonstrated

Received 2 October 2016; accepted 18 December, 2016
*E-mail: minwang@nwpu.edu.cn

that as the phase level is up to a certain number, and the wavefront manipulation efficiency would approximate to 1[38-39]. On the other hand, if the size of the nanoantenna is large, high order diffractions would become significant, leading to a deteriorated efficiency. Meanwhile, since the metasurface is low pixel, the wavefront manipulating efficiency is further decreased.

To overcome these drawbacks, the structure yielding continuous phase is considered to be the reasonable alternative[13, 40]. In this paper, the sine-shaped meanderline is emphatically introduced and investigated which applies phase profile without any interruptions. Simulation and experimental results show that intensity and number of the split beams are dependent on the phase profile brought by the proposed meanderline. Owing to the phase-geometric-dependence feature, the meanderline beam splitter operates in a broad spectrum range spanning from near-infrared to visible frequency regions. Although the discrete metasurface of phase discontinuity had been demonstrated to perform the similar function[25], the proposed meanderline exhibits some special advantages. First, the efficiency is enhanced in comparison with the metasurface of phase-discontinuity. Second, beam splitting behaviors is possible of being dynamically controlled only if the electromagnetic characteristic of the material used to make up the meanderline is external bias responded.

2 Results

Sine-shaped meanderlines are designed, fabricated and measured. At the beginning, the sine curve (the red thin line in Fig. 1(a) is broadened along y axis to form a metallic wire element with vertical width of δ, and then respectively repeated along x and y directions with periods of P and P_y, as Figs. 1(a) and 1(b) show. To prevent the diffraction in yoz plane, the value of P_y should be close to or less than the incident wavelength λ. Although the width of metallic wire w along the meanderline is not equal, scattering amplitudes are nearly uniform for a given λ due to the tiny difference ($< \lambda/70$). Sine-shaped meanderlines are fabricated by focused ion beam (Helios Nanolab 650, FEI Company) on a gold layer of 120 nm thickness, deposited on the top of a 1-mm-thick glass substrate. Figs. 1(c) and 1(d) give the scanning electron microscope (SEM) images of the two fabricated samples with a detail map of Sample 2 appending in Fig. 1(d).

Fig. 2 shows simulation and experimental results of the two samples which are displayed in left and right columns, respectively. Three bright spots appear in the view field of the CCD camera when Sample 1 is under testing, corresponding to 0 and ±1 order diffraction light beams. For Sample 2, only ±1 order diffraction light spots are observed. In order to quantitatively describe the intensity, the spectra at the center of the spot are abstracted. Three peaks are obtained with one at normal direction and the other two symmetrically located at the two sides for

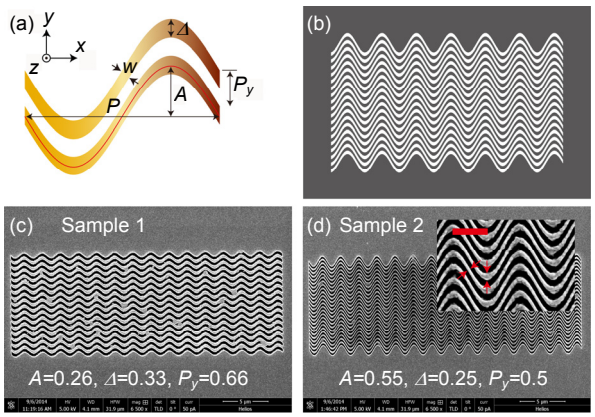

Fig.1 Design and fabrication of the sine-shaped metallic meanderlines. (a) Curve function of the thin red line is $f(x) = A\sin(\pi x)$, where A is the amplitude coefficient. The single element is formed via broadening the curve along y axis. The width of the metallic wire along meanderline is w which achieves the maximal value δ at each inflexion of the curve. Periods along x and y directions are P = 2 μm and P_y, respectively. (b) Repeating the element along x and y directions in items of the periods, we finally finish the design of the meanderline samples. SEM top images of fabricated Sample 1 (c) containing 15 × 17 periods and Sample 2 (d) composed of 15 × 25 along x and y directions. Physical parameters of the two samples are noted in the pictures. The inset in (d) shows the details of Sample 2 with the scale bar of 1 μm long. The maximal width difference along the meanderline is less than 9 nm, as the red marked arrows shows.

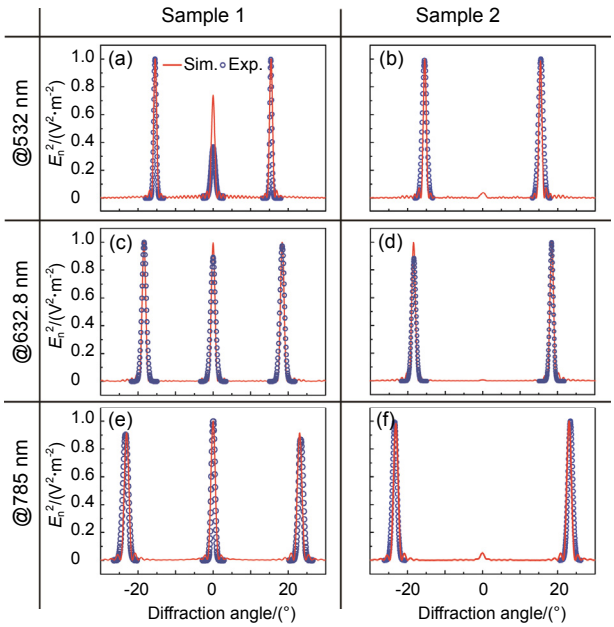

Fig.2 Simulated and measured spectra of the converted CP light. Simulations are processed with the commercial electromagnetic simulation soft of CST 2013. (a), (c), (e) show the spectra of Sample 1 and (b), (d), (f) are the results of Sample 2 at incident wavelengths of 532 nm, 632.8 nm, and 785 nm. The tiny fluctuations around the peaks in experimental data are ignored in the post processing. Intensity data below tenth of the maximum are ignored in consideration of the camera limitation, leading to the absence of the center spectra for Sample 2.

Sample 1. Diffraction angles of the anomalous light beams are ±15.5°, ±18.4°, and ±23.1° respected to normal direction at wavelengths of 532 nm, 632.8 nm, and 785 nm. Spectra of Sample 2 are similar, except the greatly suppressed 0-order diffraction light, as Figs. 2(b), 2(d), and 2(f) show. All experimental results are consistent with the simulation ones.

3 Discussion

In actual, an arbitrary spatially-variant or anisotropic transmission function produces a particular geometric phase profile corresponding to a special spectrum in wave-vector domain. Note that the geometric phase profile is regarded as an integration of phase for each x. In this paper, function $f(x) = A\sin(\pi x)$ is adopted to yield the desired phase profile. The phase change is produced when a circularly polarized (CP) light converts to its opposite state, which is simply described as $\varphi = \pm 2\zeta$, where $\zeta = \arctan(\partial f(x)/\partial x)$[7]. The sign is determined by the polarization state of the incident light, i.e. sign '+' for LCP light and sign '–' for RCP light. According to the phase profile, we can obtain spectrum of the converted CP light via the following equation:

$$I(k) = (FFT(\mathrm{e}^{\mathrm{i}\varphi(x)}))^2 = \{FFT[\exp(\mathrm{i}2\arctan(\frac{\partial f(x)}{\partial x}))]\}^2 \quad . \qquad (1)$$

In comparison with the results of the two samples, it can be easily seen that amplitude coefficient A affects the beam splitting behavior dramatically. Theoretical analysis is further carried out to reveal the basic reason in detail. Figs. 3(a) and 3(b) depict the phase profiles and the converted CP light spectra for various A values at the given wavelength of 632.8 nm. For A=0, the meanderline degenerates to a straight line grating. A uniform phase profile is yielded, resulting in the absence of beam splitting. As the value increases, the phase profile and the diffraction pattern vary. During the changing procedure, the spectrum at normal direction undergoes absence and re-presence. Actually, the intensity is enhanced to the same level of ±1 diffraction light beams when A=0.26 μm, and attenuated to zero for A=0.55 μm. In the case of A=1.06 μm, intensities of the three light beams are equal again but with stronger high order diffraction. A nearly steady tapered spectrum is obtained for arbitrary A larger than 1.5 μm because of the almost unchanged phase profile.

Since the geometric phase is wavelength-independent, we believe that the meanderline is broadband-responded. The prediction is verified in simulation at given A values of 0.26 μm and 0.55 μm. The spectra are given in Figs. 4(c) and 4(d) as a function of wavelength. Clearly, the beam splitting behavior holds from 0.1 μm to 1.8 μm covering near infrared and visible regions. Diffraction angle and wavelength follow the grating equation $\sin\theta_m = m\lambda/P$, where θ_m is the diffraction angle of the mth-order. In other words, it means that high order diffraction light beams can be avoided by increasing the incident wavelength. Relevant numerical validations are described in supporting information.

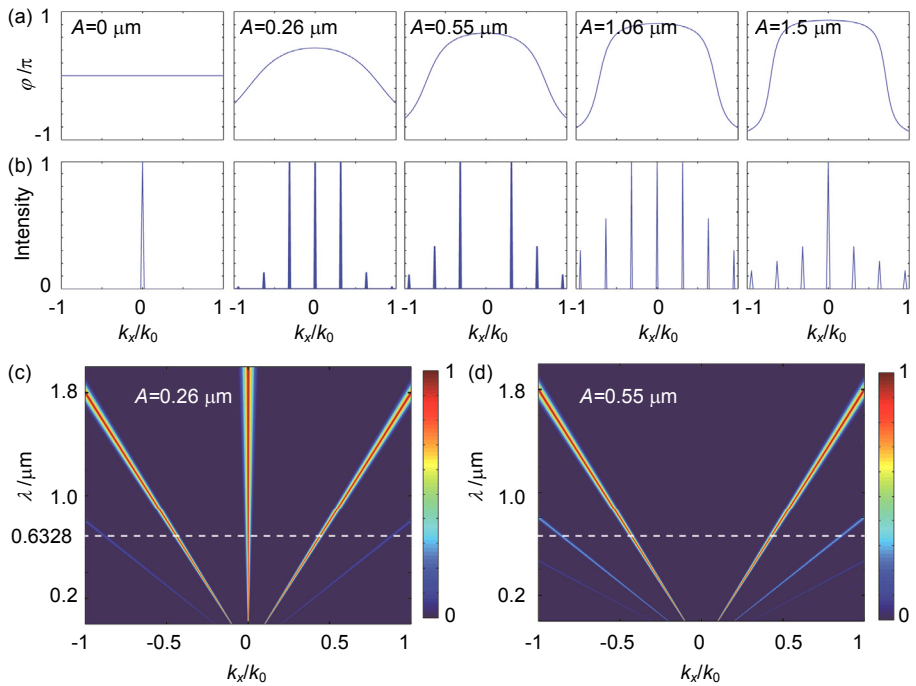

Fig.3 Effect of amplitude coefficient A on phase profile and wavefront manipulation. Phase profile in a period of the proposed sine function (a) and the corresponding converted CP light spectra (b) for various A values. Spectra as a function of incident wavelength λ and relative wave vector k_x/k_0 are given for different A values of 0.26 μm (c) and 0.55 μm (d), respectively. The broken white line is marked at the wavelength of 632.8 nm.

Besides the proposed sine-shaped structure, other mean-derlines, such as the traditional triangle and saw-tooth gratings, show similar capability of splitting the converted CP light beam due to analogous configurations. The difference is discussed in the following. Here, a simple function $g(x) = B \times |x|$ is introduced to describe the basic shape of the triangle grating, where x varies from -1 to 1 μm. Obviously, its derivative function is discontinuous and breaks at $x = 0$ in Math. Since the phases of the electric fields around the turnings are subsistent, we properly modulate the derivative function in calculation. It is explained in details by taking three-beam splitting as an example. Via equation 1, we confirm that the spectrum of $f(x)$ with $A = 0.26$ is equal to that of $g(x)$ with $B = 0.54$. Fig. 4(a) shows the phase profile of the derivative function which looks like a rectangular plus with rising (trailing) edge of 0.2 μm in half a period. Spectrum of the converted CP light at 632.8 nm is shown in Fig. 4(c). As a contrast, same items for the proposed meanderline are calculated and depicted in Figs. 4(b) and 4(d). It is clear that intensities of 0 and ±1 -orders are nearly same for the two cases. The difference is the power distribution of the high-order diffraction light beams. For the former, more energy is concentrated at ±3-orders, rather than ±2-orders. Figs. 4(e) and 4(f) show the spectra at 1050 nm. In this case, high-order diffraction light beams are suppressed and intensities are nearly equal. Thus it is concluded that the sine-shaped meanderline is nearly equal to the triangle grating in beam splitting.

Although metasurfaces of phase discontinuity can represent the splitting behavior by constructing similar phase profiles, the efficiency is usually receded. Fig. 5(a) depicts the metasurface possessing discontinuous phase profile similar to that of the triangle grating. The inset at upper right gives the dimension of the unit cell. Polarization conversion ratio from LCP to RCP light is shown in the inset of lower right. The peak is around 285.7 THz, corresponding to the wavelength of 1050 nm. Normalized spectra of the converted CP light are shown in Fig. 5(b) for 632.8 nm and 1050 nm (close to and larger than the period P_y), respectively. Fig. 5(c) shows the metasurface of which the function is 'equal to' the proposed sine-shaped meanderline. Five slits with different rotation angles in a period are used to approximate the continuous phase profile shown in Fig. 4(b). The corresponding normalized spectra are depicted in Fig. 5(d). Clearly, the diffraction angles of the anomalous light beams agree with the expectation. In contrast to the proposed meanderline, intensities of the split beams are unequal and the efficiency is lower due to the absence of some phase information.

Efficiency ratio of the three models are listed in Table 1, which is calculated by dividing the forward scattering electric field of converted CP light by the total scattering field. Clearly, the proposed meanderline is better than the discrete models in beam splitting. Simulation results validate that efficiency of the sine-shaped meanderline is 1.5 ~ 2 times than that of the discrete metasurfaces at 632.8 nm and 1050 nm. It means that the structure with continuous phase profile is more suitable than that of phase-discontinuity in some applications including beam splitting. Actually, the maximal efficiency of the proposed meanderline in theory reaches about 0.67, see supporting information. A point worth emphasizing is that the sine-shaped structure is just one example of meanderlines with continuous phase profile. One can eliminate high order diffractions to further enhance the efficiency by optimizing the configuration.

Moreover, it is inconvenient to apply a uniform bias voltage on metasurfaces composed of discontinuous nanoantenna-array. That means the wavefront manipulations of such devices are fixed once it is fabricated.

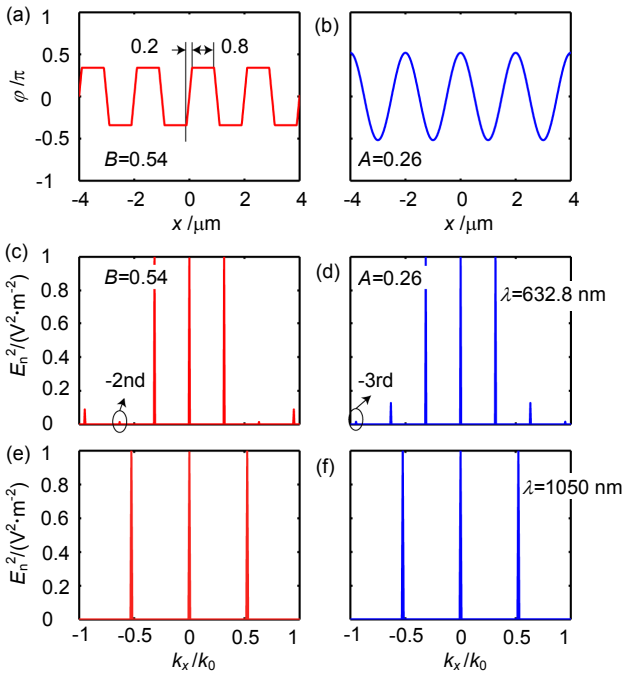

Fig.4 Wavefront manipulation of meanderlines with different phase-continuity profiles. (a) A typical phase profile of the triangle grating. We set a square-wave function with certain rising and trailing edges to mimic the phase of electric field of the triangle grating. (b) Phase profile introduced by the sine-function we proposed. (c) and (d) show the 1D spectra of the converted CP light at 632.8 nm for the two kinds of phase profiles normalized by the sine-function one. (e) and (f) are the 1D spectra at 1050 nm for the two cases.

Table 1 Efficiency comparison for the meanderline and metasurfaces of phase discontinuity

	Efficiency ratio	
	@ 632.8 nm	@ 1050 nm
Meanderline	1.0	0.823
Discrete model 1	0.477	0.444
Discrete model 2	0.556	0.485

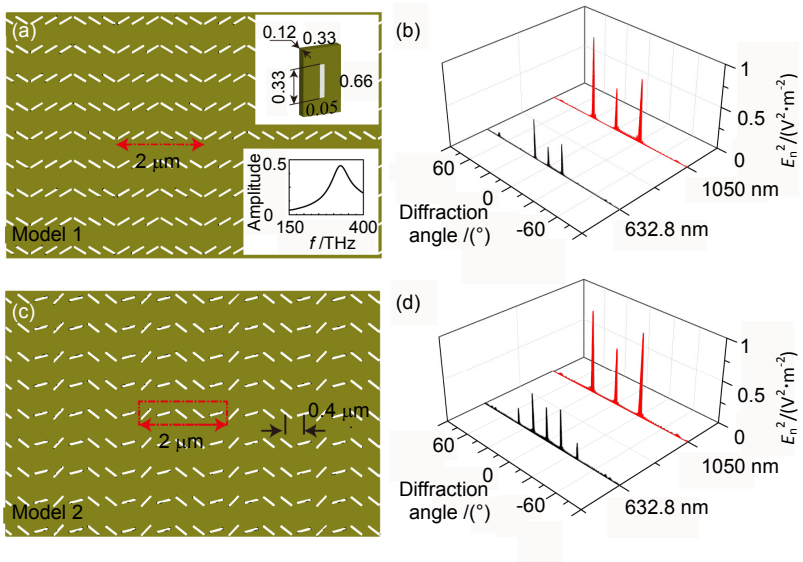

Fig.5 Metasurfaces with phase-discontinuity to realize the similar function of splitting the converted CP light beam. The structure in (a) possesses six discrete unit cells in a period to mimic the profile in Fig. 5(a). The upper inset shows the dimension of the unit cell. The lower one is the polarization conversion ratio from LCP to RCP light. The peak is around 285.7 THz. Normalized spectra at 632.8 nm and 1050 nm are depicted in (b) with diffraction angles of ±18.4° and ± 31.5°. The metasurface in (c) contains five slits with different rotation angles in a period to approximate the phase profile in Fig. 5(b). Normalized spectra of converted CP light beam are shown in (d).

However, it is feasible to tune the performance using the proposed meanderline due to its continuous configuration. Assuming that the opposite voltages are applied on the two symmetrical metallic meanderlines separated by a bias-responsible dielectric material (graphene as an example), the splitting behaviors may be dynamically controlled.

4 Methods

The experiment setup is shown in Fig. 6. The incident monochromatic beam from a He-Ne laser is converted into left-handed polarized light (LCP) by a cascaded linear polarizer (P1) and quarter-wave plate (QW1) before illuminating onto the sample. Co-polarized component of the transmitted light are eliminated by another cascaded quarter wave plate (QW2) and linear polarizer (P2) and the remaining right-handed polarized (RCP) component are collected by a charge-coupled device (CCD, WinCamD-UCD15, DataRay Inc) camera at various directions.

The Au patterns of 24-bit format BMP files were first compiled with Matlab, subsequently milled by focused ion beam (Helios Nanolab 650, FEI Company) at 3 kV acceleration voltage and 24 pA beam current. First, CP light is incident on a non-patterned Au layer at a thickness of 120 nm.

5 Conclusions

We demonstrated that continuous metasurfaces containing sine- or triangle-shaped are more efficient in splitting the converted CP light beam than the discrete metasurface with phase-discontinuity due to the avoidance of the unwanted higher-order diffraction. The proposed sine-shaped meanderlines are capable of splitting the converted CP light into several beams with equal intensities at visible and infrared regions, similar to the traditional grating. Moreover, anticipated improvements including efficiency enhancement and agile tunability give them the opportunity in applying in optical communications, imaging and other phase-relative techniques.

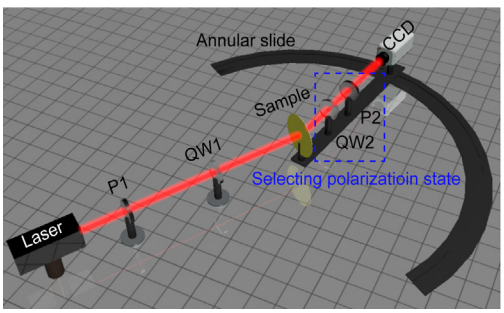

Fig.6 Schematic of the optical set-up for beam splitting measurement. An input beam from a laser source is adjusted to be left-handed circularly polarized (LCP) after a horizontal direction polarizer (P1) and a 45° rotated quarter-wave plate (QW1), and then impinges on the sample. Light beams with opposite-handed component, i.e. RCP, are picked out using a cascaded horizontal direction quarter-wave (QW2) plate and polarizer (P2) fixed on a metallic arm connecting to a semi-annular slide rail with radius of 30 cm, and finally received by a CCD camera moving along the slide rail.

Acknowledgements

This work was supported by National Natural Science Funds (61601367, 61601375) and the Fundamental Research Funds for the Central Universities (3102016 ZY028).

References

1 Yu Nanfang, Capasso F. Flat optics with designer metasurfaces [J]. *Nature Materials*, 2014, **13**(2): 139–150.

2 O'Shea D C, Suleski T J, Kathman A D, *et al*. Diffractive Optics: Design, Fabrication, and Test[M]. Bellingham, WA: SPIE Press, 2003.

3 Luo Xiangang, Pu Mingbo, Ma Xiaoliang, *et al*. Taming the electromagnetic boundaries via metasurfaces: from theory and fabrication to functional devices[J]. *International Journal of Antennas and Propagation*, 2015, **2015**: 204127.

4 Yu N F, Genevet P, Kats M A, *et al.* Light propagation with phase discontinuities: generalized laws of reflection and refraction[J]. *Science*, 2011, **334**(6054): 333–337.

5 Yang Y, Wang W, Moitra P, *et al.* Dielectric meta-reflectarray for broadband linear polarization conversion and optical vortex generation[J]. *Nano Letters*, 2014, **14**(3): 1394–1399.

6 Pu Mingbo, Chen Po, Wang Yanqin, *et al.* Anisotropic meta-mirror for achromatic electromagnetic polarization manipulation[J]. *Applied Physics Letters*, 2013, **102**(13): 131906.

7 Pu Mingbo, Zhao Zeyu, Wang Yanqin, *et al.* Spatially and spectrally engineered spin-orbit interaction for achromatic virtual shaping[J]. *Scientific Reports*, 2015, **5**: 9822.

8 Huang Lingling, Chen Xianzhong, Bai Benfang, *et al.* Helicity dependent directional surface plasmon polariton excitation using a metasurface with interfacial phase discontinuity[J]. *Light*: *Science & Applications*, 2013, **2**(3): e70.

9 Pelzman C, Cho S Y. Polarization-selective optical transmission through a plasmonic metasurface[J]. *Applied Physics Letters*, 2015, **106**(25): 251101.

10 Zhao Zeyu, Pu Mingbo, Gao Hui, *et al*. Multispectral optical metasurfaces enabled by achromatic phase transition[J]. *Scientific Reports*, 2015, **5**: 15781.

11 Alali F, Kim Y H, Baev A, *et al.* Plasmon-enhanced metasurfaces for controlling optical polarization[J]. *ACS Photonics*, 2014, **1**(6): 507–515.

12 Shaltout A, Liu Jingjing, Shalaev V M, *et al.* Optically active metasurface with non-chiral plasmonic nanoantennas[J]. *Nano Letters*, 2014, **14**(8): 4426–4431.

13 Pu Mingbo, Li Xiong, Ma Xiaoliang, *et al.* Catenary optics for achromatic generation of perfect optical angular momentum[J]. *Science Advances*, 2015, **1**(9): e1500396.

14 Aieta F, Genevet P, Yu Nanfang, *et al.* Out-of-plane reflection and refraction of light by anisotropic optical antenna metasurfaces with phase discontinuities[J]. *Nano Letters*, 2012, **12**(3): 1702–1706.

15 Pu Mingbo, Chen Po, Wang Changtao, *et al.* Broadband anomalous reflection based on gradient low-Q meta-surface[J]. *AIP Advance*, 2013, **3**(5): 052136.

16 Ni Xingjie, Emani N K, Kildishev A V, *et al.* Broadband light bending with plasmonic nanoantennas[J]. *Science*, 2012, **335**(6067): 427.

17 Pors A, Albrektsen O, Radko I P, *et al.* Gap plasmon-based metasurfaces for total control of reflected light[J]. *Scientific Reports*, 2013, **3**: 2155.

18 Ma Xiaoliang, Pu Mingbo, Li Xiong, *et al.* A planar chiral meta-surface for optical vortex generation and focusing[J]. *Scientific Reports*, 2015, **5**: 10365.

19 Yu Nanfang, Aieta F, Genevet P, *et al.* A broadband, background-free quarter-wave plate based on plasmonic metasurfaces[J]. *Nano Letters*, 2012, **12**(12): 6328–6333.

20 Li Xiong, Pu Mingbo, Wang Yanqin, *et al*. Dynamic control of the extraordinary optical scattering in semicontinuous 2D metamaterials[J]. *Advanced Optical Materials*, 2016, **4**(5): 659–663.

21 Guo Yinghui, Yan Lianshan, Pan Wei, *et al*. Scattering engineering in continuously shaped metasurface: an approach for electromagnetic illusion[J]. *Scientific Reports*, 2016, **6**: 30154.

22 Hu Dan, Wang Xinke, Feng Shengfei, *et al*. Ultrathin terahertz planar elements[J]. *Advanced Optical Materials*, 2013, **1**(2): 186–191.

23 Aieta F, Genevet P, Kats M A, *et al.* Aberration-free ultrathin flat lenses and axicons at telecom wavelengths based on plasmonic metasurfaces[J]. *Nano Letters*, 2012, **12**(9): 4932–4936.

24 Chen Xianzhong, Huang Lingling, Mühlenbernd H, *et al.* Dual-polarity plasmonic metalens for visible light[J]. *Nature Communications*, 2012, **3**: 1198.

25 Chen Xianzhong, Zhang Yan, Huang Lingling, *et al*. Ultrathin metasurface laser beam shaper[J]. *Advanced Optical Materials*, 2014, **2**(10): 978–982.

26 He J W, Ye J S, Wang X K, *et al.* A broadband terahertz ultrathin multi-focus lens[J]. *Scientific Reports*, 2016, **6**: 28800.

27 Zhao Yang, Alù A. Tailoring the dispersion of plasmonic nanorods to realize broadband optical meta-waveplates[J]. *Nano Letters*, 2013, **13**(3): 1086–1091.

28 Zhang Xiaohu, Jin Jinjin, Wang Yanqin, *et al.* Metasurface-based broadband hologram with high tolerance to fabrication errors[J]. *Scientific Reports*, 2016, **6**: 19856.

29 Ni Xingjie, Kildishev A V, Shalaev V M. Metasurface holograms for visible light[J]. *Nature Communications*, 2013, **4**: 2807.

30 Chen Weiting, Yang Kuangyu, Wang C M, *et al.* High-efficiency broadband meta-hologram with polarization-controlled dual images[J]. *Nano Letters*, 2014, **14**(1): 225–230.

31 Zheng Guoxing, Mühlenbernd H, Kenney M, *et al.* Metasurface holograms reaching 80% efficiency[J]. *Nature Nanotechnology*, 2015, **10**(4): 308–312.

32 Lin Jiao, Mueller J P B, Wang Qian, *et al.* Polarization-controlled tunable directional coupling of surface plasmon polaritons[J]. *Science*, 2013, **340**(6130): 331–334.

33 Yin Xiaobo, Ye Ziliang, Rho J, *et al.* Photonic spin hall effect at metasurfaces[J]. *Science*, 2013, **339**(6126): 1405–1407.

34 Ma Guancong, Yang Min, Xiao Songwen, *et al*. Acoustic metasurface with hybrid resonances[J]. *Nature Materials*, 2014, **13**(9): 873–878.

35 Li Yong, Jiang Xue, Li Ruiqi, *et al.* Experimental realization of full control of reflected waves with subwavelength acoustic metasurfaces[J]. *Physical Review Applied*, 2014, **2**(6): 064002.

36 Werner D H, Kwon D H. Transformation Electromagnetics and Metamaterials: Fundamental Principles and Applications[M]. London: Springer, 2014.

37 Luo Xiangang. Principles of electromagnetic waves in metasurfaces[J]. *Science China Physics*, *Mechanics & Astronomy*, 2015, **58**(9): 594201.

38 Ding X, Monticone F, Zhang K, *et al.* Ultrathin pancharatnam-berry metasurface with maximal cross-polarization efficiency[J]. *Advanced Materials*, 2015, **27**: 1195–1200.

39 Aieta F, Genevet P, Kats M, *et al*. Aberrations of flat lenses and aplanatic metasurfaces[J]. *Optics Express*, 2013, **21**(25): 31530–31539.

40 Zhang Lei, Hao Jiaming, Qiu Min, *et al.* Anomalous behavior of nearly-entire visible band manipulated with degenerated image dipole array[J]. *Nanoscale*, 2014, **6**(21): 12303–12309.